Correction

BIOPHYSICS AND COMPUTATIONAL BIOLOGY

Correction for "A posttranslational modification of the mitotic kinesin Eg5 that enhances its mechanochemical coupling and alters its mitotic function" by Joseph M. Muretta, Babu J. N. Reddy, Guido Scarabelli, Alex F. Thompson, Shashank Jariwala, Jennifer Major, Monica Venere, Jeremy N. Rich, Belinda Willard, David D. Thomas, Jason Stumpff, Barry J. Grant, Steven P. Gross, and Steven S. Rosenfeld, which was first published February 5, 2018; 10.1073/pnas.1718290115 (*Proc Natl Acad Sci USA* 115:E1779–E1788).

The authors note that the affiliation for Alex F. Thompson should instead appear as Department of Molecular Physiology and Biophysics, University of Vermont, Burlington, VT 05405. The corrected author and affiliation lines appear below. The online version has been corrected.

Joseph M. Muretta[a], Babu J. N. Reddy[b,c], Guido Scarabelli[d], Alex F. Thompson[e], Shashank Jariwala[d], Jennifer Major[f], Monica Venere[g], Jeremy N. Rich[e], Belinda Willard[f], David D. Thomas[a], Jason Stumpff[e], Barry J. Grant[h], Steven P. Gross[b,c], and Steven S. Rosenfeld[i]

[a]Department of Biochemistry, Molecular Biology, and Biophysics, University of Minnesota, Minneapolis, MN 55455; [b]Department of Developmental and Cell Biology, University of California, Irvine, CA 92697; [c]Department of Physics, University of California, Irvine, CA 92697; [d]Department of Computational Medicine and Bioinformatics, University of Michigan, Ann Arbor, MI 48109; [e]Department of Molecular Physiology and Biophysics, University of Vermont, Burlington, VT 05405; [f]Department of Cancer Biology, Lerner Research Institute of the Cleveland Clinic Foundation, Cleveland, OH 44195; [g]Department of Radiation Oncology, Ohio State University, Columbus, OH 43210; [h]Division of Biological Sciences, Section of Molecular Biology, University of California, San Diego, La Jolla, CA 92093; and [i]Department of Medical Oncology, Mayo Clinic, Jacksonville, FL 32224

Published online March 5, 2018.

www.pnas.org/cgi/doi/10.1073/pnas.1802910115

CORRECTION

A posttranslational modification of the mitotic kinesin Eg5 that enhances its mechanochemical coupling and alters its mitotic function

Joseph M. Muretta[a,1], Babu J. N. Reddy[b,c,1], Guido Scarabelli[d,1], Alex F. Thompson[e,1], Shashank Jariwala[d], Jennifer Major[f], Monica Venere[g], Jeremy N. Rich[e], Belinda Willard[f], David D. Thomas[a], Jason Stumpff[e], Barry J. Grant[h], Steven P. Gross[b,c], and Steven S. Rosenfeld[i,2]

[a]Department of Biochemistry, Molecular Biology, and Biophysics, University of Minnesota, Minneapolis, MN 55455; [b]Department of Developmental and Cell Biology, University of California, Irvine, CA 92697; [c]Department of Physics, University of California, Irvine, CA 92697; [d]Department of Computational Medicine and Bioinformatics, University of Michigan, Ann Arbor, MI 48109; [e]Department of Molecular Physiology and Biophysics, University of Vermont, Burlington, VT 05405; [f]Department of Cancer Biology, Lerner Research Institute of the Cleveland Clinic Foundation, Cleveland, OH 44195; [g]Department of Radiation Oncology, Ohio State University, Columbus, OH 43210; [h]Division of Biological Sciences, Section of Molecular Biology, University of California, San Diego, La Jolla, CA 92093; and [i]Department of Medical Oncology, Mayo Clinic, Jacksonville, FL 32224

Edited by Thomas D. Pollard, Yale University, New Haven, CT, and approved January 5, 2018 (received for review October 20, 2017)

Numerous posttranslational modifications have been described in kinesins, but their consequences on motor mechanics are largely unknown. We investigated one of these—acetylation of lysine 146 in Eg5—by creating an acetylation mimetic lysine to glutamine substitution (K146Q). Lysine 146 is located in the α2 helix of the motor domain, where it makes an ionic bond with aspartate 91 on the neighboring α1 helix. Molecular dynamics simulations predict that disrupting this bond enhances catalytic site–neck linker coupling. We tested this using structural kinetics and single-molecule mechanics and found that the K146Q mutation increases motor performance under load and coupling of the neck linker to catalytic site. These changes convert Eg5 from a motor that dissociates from the microtubule at low load into one that is more tightly coupled and dissociation resistant—features shared by kinesin 1. These features combined with the increased propensity to stall predict that the K146Q Eg5 acetylation mimetic should act in the cell as a "brake" that slows spindle pole separation, and we have confirmed this by expressing this modified motor in mitotically active cells. Thus, our results illustrate how a posttranslational modification of a kinesin can be used to fine tune motor behavior to meet specific physiological needs.

kinesin | acetylation | mitosis | molecular motor

Members of the kinesin superfamily of molecular motors fulfill specific roles in cell physiology. Some serve as transporters, others serve as regulators of microtubule (MT) dynamics, and others still serve as mitotic motors (1–4). Nevertheless, individual kinesins can play multiple cellular roles. For example, while kinesin 1 transports organelles, it also slides MTs during axonal elongation (5). MCAK, an MT-depolymerizing mitotic kinesin, can also drive cell motility (6). MTs also play multiple roles in cell physiology, and this adaptability is due in part to multiple posttranslational modifications (PTMs) (7–9). Thus, some of the multifunctionality of kinesin motors might reflect PTMs that modify their mechanochemical behavior. PTMs have been identified in most kinesins, including many in the catalytic domain of these enzymes (10, 11). However, in nearly all cases, the consequences of these PTMs on motor function remain unknown. Multiple PTMs in the motor domain of the mitotic kinesin Eg5 have been reported (12), including in Loop 5 and helices α2 and α3—all in the vicinity of the catalytic site (Fig. 1*A*). As with other kinesins, Eg5 also plays multiple roles in cell physiology, including not only formation of the mitotic spindle in dividing cells but also, axonal branching and cell motility (13, 14). These roles may be associated with distinct mechanochemical requirements—which might be achieved via specific PTMs. One such PTM of Eg5 is acetylation of a lysine residue (K146) at the C-terminal end of helix α2 (Fig. 1*A*) (15–17). Lysine 146 makes a salt bridge to aspartate 91 on helix α1, and its acetylation disrupts this ionic interaction—an effect that can be mimicked by a lysine to glutamine point mutation (18–20). The importance of acetylation in cell biology is underscored by the recent findings that it regulates not only chromatin activity through its effects on histones (21) but also, transcription, metabolism, autophagy, and viral infection (22–25).

Two key structural domains in kinesin 1 and Eg5—switch 1 (Sw1) and the neck linker (NL)—alternate between two orientations during the ATPase cycle (26–30). Sw1 senses the γ-phosphate of ATP, and it assumes "open" (capable of binding ATP) and "closed" (capable of hydrolyzing ATP) conformations. The NL moves in response to ATP binding between "undocked" (not force-generating) and "docked" (force-generating) orientations. We found that, while Sw1 and the NL are tightly coupled in kinesin 1 (e.g., closed Sw1 associated with docked NL), they are more loosely coupled in Eg5. Tight coupling is important for

Significance

Members of the kinesin superfamily serve a wide variety of functions, and a dominant narrative for these molecular motors has been that each member of the superfamily is uniquely specialized to serve a very limited set of functions. However, it is now appreciated that many members of this group serve several distinct physiological roles, and it has been unclear how these kinesins accomplish this functional flexibility. In this report, we describe a posttranslational modification of the kinesin 5 family member Eg5 that dramatically alters its chemomechanical behavior to make it function much more efficiently under load and in ensembles. This work provides the biophysical context required to mechanistically understand the effects of modified Eg5 in dividing cells.

Author contributions: J.M.M., B.J.N.R., G.S., A.F.T., S.J., J.M., M.V., B.W., J.S., B.J.G., S.P.G., and S.S.R. designed research; J.M.M., B.J.N.R., G.S., A.F.T., S.J., J.M., B.W., J.S., B.J.G., S.P.G., and S.S.R. performed research; J.M.M., B.J.N.R., G.S., A.F.T., S.J., J.N.R., D.D.T., J.S., B.J.G., S.P.G., and S.S.R. contributed new reagents/analytic tools; J.M.M., B.J.N.R., G.S., A.F.T., S.J., B.W., J.S., B.J.G., S.P.G., and S.S.R. analyzed data; and J.M.M., B.J.N.R., J.S., B.J.G., S.P.G., and S.S.R. wrote the paper.

The authors declare no conflict of interest.

This article is a PNAS Direct Submission.

[1]J.M.M., B.J.N.R., G.S., and A.F.T. contributed equally to this work.

[2]To whom correspondence should be addressed. Email: rosenfeld.steven@mayo.edu.

This article contains supporting information online at www.pnas.org/lookup/suppl/doi:10.1073/pnas.1718290115/-/DCSupplemental.

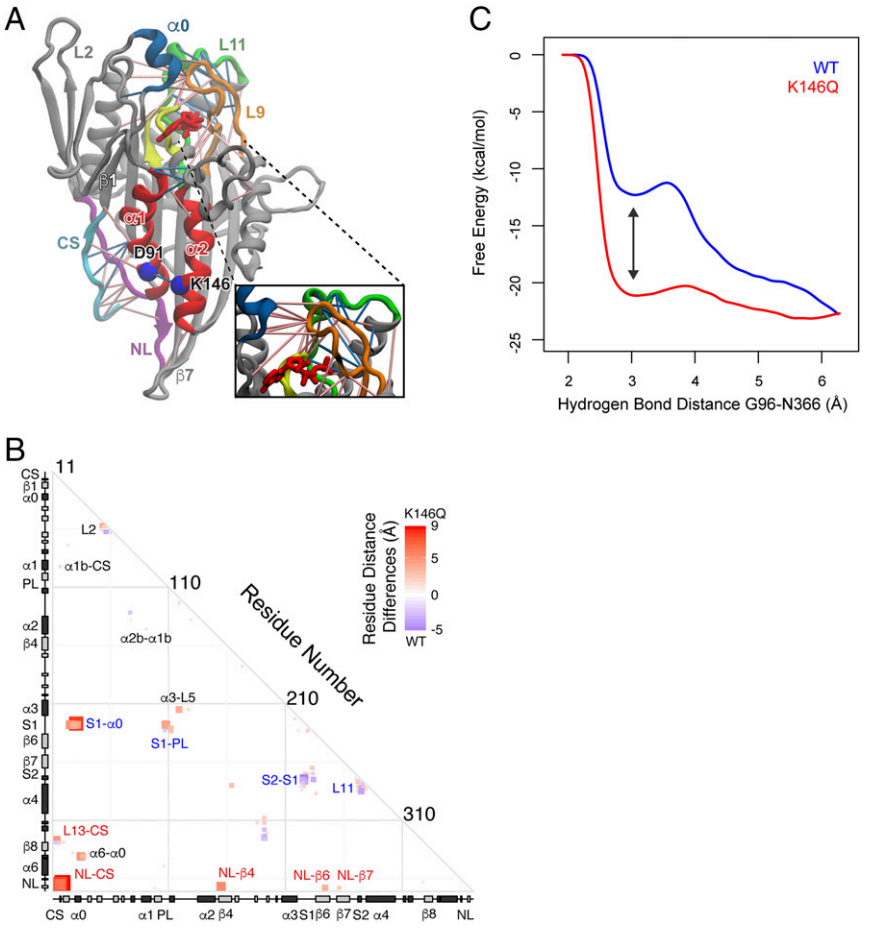

Fig. 1. MD simulations of the effect of the K146Q acetylation mimetic mutation. (*A*) Molecular structure of Eg5 highlighting major structural elements, including Loop 9/Sw1 (orange), Loop 11/Sw2 (green), P loop (yellow), helix α0 (blue), NL (purple), CS (cyan), and helices α1 and α2 (red). Also shown is the WT salt bridge residue pair D91 and K146 (as bright blue spheres). Significant ($P < 0.05$) residue–residue distance changes between WT and K146Q mutant simulations are displayed as red and blue lines, with color intensity representing the magnitude of change and matching that in *B*. (*Inset*) Enlarged view of the catalytic site. (*B*) Pairwise residue difference distance analysis of WT and K146Q simulations. Significant ($P < 0.05$) residue–residue distance changes are displayed with size and color intensity scaled by magnitude (red for shorter in K146Q and blue for shorter in the WT). Major secondary structure elements are displayed in the marginal plot regions (α-helices in black and β-strands in gray). Specific structural regions noted in the text with distinct interactions with the NL and Sw1 regions have been labeled in red and blue, respectively. (*C*) Free energy profile from well-tempered metadynamics simulations for NL docking/undocking of WT (blue) and K146Q mutant (red) as a function of the distances between residues N366 (NL) and G96 (helix α1). The arrow denotes the energy difference between the WT and K146Q at point of hydrogen bond formation.

a highly processive motor that operates in isolation, such as kinesin 1, as it helps ensure that the motor does not enter a weak MT binding state before it has docked its NL and generated force. Conversely, this might be unnecessary for Eg5, which by working in large ensembles, may not need to be highly processive. Here, we have focused on the acetylation of K146 through molecular dynamics (MD) simulations, transient time-resolved kinetics, single-molecule mechanics, and time-lapse microscopy of cells in mitosis. We find that a pseudoacetylation mutant of Eg5 (K146Q) shows much tighter conformational coupling of Sw1 to the NL, and this is associated with improved motor performance under load—features characteristic of kinesin 1. Taken together, our results suggest that kinesin PTMs can act as a "molecular gear shift"—broadening a specific kinesin's capabilities and enhancing the flexibility that a cell has to respond to a wide variety of physiological demands.

Results

The K146Q Acetylation Mimetic Has Little Effect on Enzymatic Turnover, Nucleotide Binding, or MT Dissociation. We examined the consequences of the K146Q mutation on the steady-state enzymology of Eg5 by using a cysteine light Eg5 motor domain monomer, referred to as $Eg5_{NL}$, which contains the WT lysine residue at position 146 as well as reactive cysteines in the NL and β-core. We previously reported that the behavior of $Eg5_{NL}$ was nearly identical to a WT Eg5 monomer with regard to (*i*) the steady-state ATPase parameters (k_{cat}, $K_{0.5,MT}$, $K_{0.5,ATP}$); (*ii*) the kinetics of ATP ($k_{b,ATP}$) and ADP ($k_{b,ADP}$) binding as measured by the fluorescent nucleotide analogs 2′-deoxy 3′-mant ATP (2′dmT) and 2′-deoxy 3′-mant ADP; (*iii*) the kinetics of ATP- and ADP-induced MT dissociation ($k_{d,ATP}$, $k_{d,ADP}$); and (*iv*) the force–velocity relationship measured at the single-molecule level (26). Here, we mutated lysine 146 to glutamine to generate the corresponding pseudoacetylated species referred to in this text as $Eg5_{NL}$K146Q. We found that the values of k_{cat}, $K_{0.5,MT}$, and $K_{0.5,ATP}$ for the $Eg5_{NL}$ and $Eg5_{NL}$K146Q at 20 °C are very similar to each other (*SI Appendix*, Fig. S1 *A* and *B* and Table S1). The rate constants for ATP binding to and release from $Eg5_{NL}$ and $Eg5_{NL}$K146Q are within 50% of each other at 20 °C and are nearly identical at 10 °C, where the binding of 2′dmT is slower and can be measured more accurately (*SI Appendix*, Fig. S1*C* and Table S1). The maximum rate for ADP binding to $Eg5_{NL}$K146Q is

354 ± 108 s^{-1} at 20 °C (*SI Appendix*, Table S1). Although the corresponding experiment was not performed on $Eg5_{NL}$, prior experiments on a cysteine free Eg5 monomer that is nearly identical to $Eg5_{NL}$ also show a very rapid rate constant for ADP binding (>>150 s^{-1}) (31).

ATP binding to Eg5 produces a conformational change in the catalytic site, and the K146Q mutation has little effect on this process. However, this local conformational change produces secondary effects transmitted through the motor domain that alter MT binding and NL orientation (32–34). We, therefore, performed MD simulations to obtain an unbiased assessment of what the global effects of the K146Q mutation might to be.

MD Simulations Predict That the K146Q Acetylation Mimetic Enhances NL Docking, Catalytic Site Closure, and the Coupling Between These Two Regions. We performed four replicate 300-ns MD simulations of WT and K146Q Eg5 complexed with ADP and bound to tubulin heterodimers. Analysis across replicates was used to predict statistically significant differences in residuewise interactions and energetics. Significant changes in residue–residue interactions associated with the K146Q mutation are evident for two functionally important domains. The first involves structures that are responsible for generating the "power stroke," and they include the NL, the cover strand (CS), Loop 13, and β7 (Fig. 1 *A* and *B*). The K146Q mutation shortens distances and enhances interactions between the CS and the NL, the CS and Loop 13, and the NL and β7. These changes are summarized in Fig. 1*B*, red labels and *SI Appendix*, Tables S2 and S3. Other charged residue interactions, including those between E14 (CS) and E92 (α1), the N-terminal portion of β1 with the neighboring Loop 13/β8, and E20 (β1) to R329 (Loop 13), are also enhanced (*SI Appendix*, Table S2). In aggregate, these explain why we find that the NL spends a significantly greater proportion of time in the docked orientation in the mutant compared with the WT (72% of simulation frames vs. 40%, respectively) (*SI Appendix*, Fig. S2*A*), and they are a consequence of the small displacements of α1 that result from removing the salt bridge between D91 (α1) and K146 (α2b). Thus, while the average distance between K146 and D91 is 3.6 ± 1.5 Å in WT Eg5, the corresponding Q146 to D91 distance in the K146Q mutant is 4.9 ± 1.2 Å, with a corresponding 5.3 kcal/mol decrease in interaction energy (*SI Appendix*, Tables S2 and S3).

The second domain includes structures that bind and coordinate nucleotide, including Loop 9/Sw1, the P loop, β1/helix α0, and Loop 14 (Fig. 1*A*). The largest change is seen for Loop 9/Sw1. The closed conformation for this loop, which is necessary for ATP hydrolysis, is more frequently seen in the mutant (75% of simulation time vs. 18%, respectively), and this leads to shorter average distances to the P loop illustrated by a decrease in the G108 (P loop) to N229 (Sw1) distance of 3 Å. Distances between Sw1 and Sw2 and between Sw1 and Loop 14/α6 also decrease in the mutant (Fig. 1*B*, blue labels and *SI Appendix*, Table S2). The K146Q mutation also causes the α0 helix to move away from Loop 2a and toward Sw1, Loop 14, and α6 (*SI Appendix*, Fig. S2*B*). Other interresidue distances, including W127 (Loop 5) to E215 (α3), D118 (Loop 5) to bound nucleotide, and D186 (Loop 8) to R312 (Loop 12), are also significantly shorter in the mutant (*SI Appendix*, Table S2). Additional simulations of acetyl lysine at position 146 revealed equivalent enhanced catalytic site closure, with the Sw1 region exhibiting a closed conformation for 70% of simulation time vs. 18% for the WT, and less dramatic but still significant ($P < 0.05$) α1, α2b, and NL distance differences leading to enhanced docking of the NL (71% of simulation time vs. 18% in the WT). Overall, these results indicate that the K146Q mutation results in dynamic perturbations both locally—reflected in an increase in the α1 to α2 distance—and at more distant functional regions, which they seem to collectively enhance coordination of the structural states of the NL with Sw1 regions.

Metadynamics simulations were used to further probe the energetic effects of the K146Q mutation on NL docking. Residue G96 at the C-terminal end of α1 forms a hydrogen bond with residue N366 in the NL, and this interaction is important for NL docking in kinesin 1 (35). We, therefore, chose the G96–N366 distance as a collective variable for characterizing the free energy of NL docking via 700-ns metadynamic simulations (Fig. 1*C*). The resulting free energy profiles indicate that the K146Q mutation favors formation of this hydrogen bond compared with the WT, with a relative total system free energy difference of 8.8 kcal/mol for docked vs. undocked (Fig. 1*C*, arrow). This predicts that NL docking should be energetically more favorable in the K146Q mutant and further highlights the structural importance of the salt bridge between α1 and α2b for modulating NL docking. Taken together, our simulations imply that a major consequence of K146 acetylation is enhanced conformational coupling between Sw1 and the NL. In our previous study (26), we showed that we could measure how conformational coupling between Sw1 and the NL changes during the motor mechanochemical ATPase cycle through use of a combination of transient kinetics and time-resolved FRET (TR^2FRET). We, therefore, applied this technique to experimentally test the predictions made by MD.

TR^2FRET Measures the Kinetics and Thermodynamics of NL Docking and Sw1 Closure in Eg5. In our prior study (26), we used TR^2FRET to measure the transient changes in mole fraction of docked NL and closed Sw1 for Eg5 and kinesin 1 that occur after mixing with nucleotide. We found that, while NL docking and Sw1 closure are tightly coupled in kinesin 1, they are less so in Eg5—a finding that explains many of the functional differences between these two motors. Our MD studies suggest that the K146Q mutation enhances the conformational coupling of the NL to Sw1 in a manner reminiscent of kinesin 1. We, therefore, generated two monomeric Eg5 constructs, each containing the K146Q mutation, that have pairs of reactive cysteines for labeling with an FRET donor [*N*-acetylaminoethyl-8-naphthylamine-1-sulfonate (AEDANS)] and acceptor [*N*-(4-dimethylamino-3,5-dinitrophenyl)maleimide (DDPM)]. The first, $Eg5_{NL}$K146Q, has been described above. The second, $Eg5_{Sw1}$K146Q, has reactive cysteines in the Sw1 loop (residue 228) and in a reference point (residue 30) along with the K146Q acetylation mimetic substitution.

We mixed donor only (AEDANS)- or donor + acceptor (AEDANS/DDPM)-labeled $Eg5_{NL}$K146Q and $Eg5_{Sw1}$K146Q + MTs with ATP in the stopped flow and then acquired TR^2FRET waveforms during subsequent ATP binding, hydrolysis, and MT dissociation. Fig. 2 illustrates representative waveforms for MT complexes of $Eg5_{NL}$K146Q (Fig. 2*A*) and $Eg5_{Sw1}$K146Q (Fig. 2*B*) after mixing with 2 mM ATP. As in our prior study (26), we performed our experiments at 10 °C to observe all phases of the resulting fluorescence transients. The acquired waveforms were analyzed as described previously (26) to determine the mole fractions of docked vs. undocked NL in $Eg5_{NL}$K146Q and closed vs. open Sw1 in $Eg5_{Sw1}$K146Q as a function of time after mixing with ATP (Fig. 2 *C* and *D*, respectively). The mole fraction transients for $Eg5_{NL}$K146Q were fit by minimal multiexponential functions, and the dependence of the rate constants and pre-exponential amplitudes were evaluated as a function of [ATP] or [ADP] (summarized in *SI Appendix*, Table S4). The mole fraction transients for $Eg5_{Sw1}$K146Q were modeled by kinetic simulation (described below) as in our previous work (26).

In $Eg5_{NL}$, both ATP binding and subsequent hydrolysis induce NL docking, and we find that the same is true for $Eg5_{NL}$K146Q. However, the K146Q mutation does alter NL movement in two ways. First, it accelerates NL docking during the ATP binding step threefold (Fig. 2*E* and *SI Appendix*, Table S4). Second, it increases the fraction of motors that dock their NL during this step from 50 to 76% (*SI Appendix*, Table S4). Combined, these effects should make force production more rapid and complete

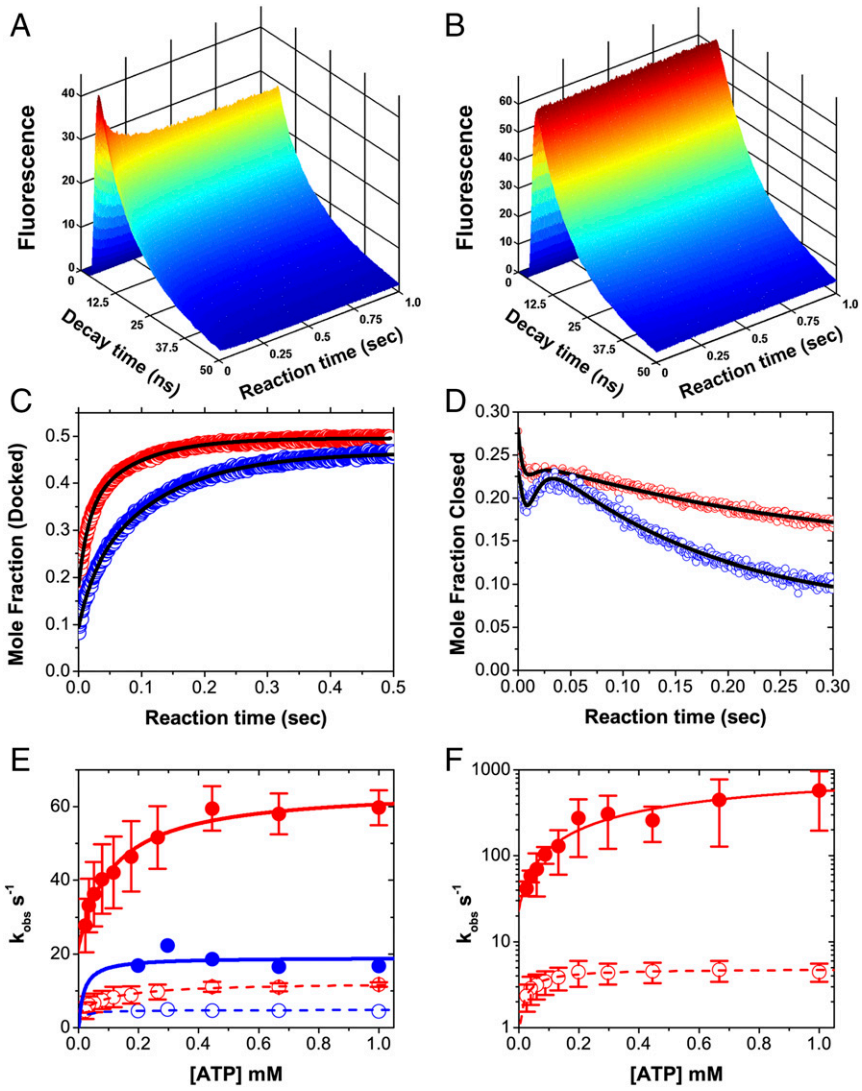

Fig. 2. TR^{2}FRET of ATP binding to rigor Eg5K146 or Eg5K146Q bound to MTs. (*A* and *B*) Representative waveforms after mixing 2 mM ATP with 1 μM AEDANS/DDPM-labeled $Eg5_{NL}$K146Q (*A*) or $Eg5_{Sw1}$K146Q (*B*) bound to 2.5 μM MTs. (*C* and *D*) Mole fraction of docked NL (*C*) or closed Sw1 (*D*) for MT-bound K146 (blue) or K146Q (red) samples as in *A* and *B*. Data in *C* were fit by biexponential functions (black lines), while data in *D* were fit by a sequential four-step kinetic mechanism described in the text. (*E*) Rate constant vs. [ATP] for the fast (closed) and slow (open) phases of biexponential fits to mole fraction transients as in *C* for $Eg5_{NL}$K146 (blue) or $Eg5_{NL}$K146Q (red). (*F*) Rate constant vs. [ATP] for the fast phase (closed) of the mole fraction transients as in *D* for $Eg5_{Sw1}$K146Q fit by a single-exponential function over the first 50 ms or a single-exponential function over a range from 50 to 300 ms. Data in *E* and *F* are fit to hyperbolic functions summarized in *SI Appendix*, Table S4. Conditions: 25 mM Hepes, pH 7.50, 50 mM potassium acetate, 5 mM magnesium acetate, 1 mM EGTA, 10 °C (n = 3–9).

with initial ATP binding. In our prior study, we also found that ATP binding alters the conformation of Sw1 by means of a four-step kinetic scheme (26):

$$M_c \underset{k_{-1}}{\overset{k_1}{\rightleftharpoons}} M_o \overset{ATP,\ K_{ATP}\cdot k_2}{\underset{k_2}{\rightleftharpoons}} M_o{\bullet}T \underset{k_{-3}}{\overset{k_3}{\rightleftharpoons}} M_c{\bullet}D{\bullet}P_i \underset{k_{-4}}{\overset{k_4}{\rightleftharpoons}} M_o{\bullet}D{\bullet}P_i$$

where M stands for the MT-bound motor; subscripts c and o stand for closed and open Sw1 conformations, respectively; T is ATP; D is ADP; and P_i is inorganic phosphate. We were able to fit our data for both Eg5 and kinesin 1 by assuming (*i*) that both closed and open Sw1 conformations are populated in the absence of nucleotide and are in rapid equilibrium; (*ii*) that ATP only binds to the open state; (*iii*) that ATP hydrolysis requires Sw1 to close; and (*iv*) that phosphate release is associated with Sw1 reopening. *SI Appendix*, Table S5 summarizes the values of the rate constants that we extracted from this simulation for kinesin 1 and for WT Eg5 ("$Eg5_{Sw1}$"). One of the major differences between Eg5 and kinesin 1 is in the value of K_4, the equilibrium constant for Sw1 reopening after ATP hydrolysis, which is nearly 10-fold larger in Eg5 than in kinesin 1. This implies that, after hydrolysis, the open and closed conformations of Sw1 in Eg5 are in a slow equilibrium that markedly favors the open state, while in kinesin 1, they are in a more rapid equilibrium, where both open and closed states are roughly equally populated. When we applied our simulation to fit the corresponding data for $Eg5_{Sw1}$K146Q (Fig. 2*D* and *SI Appendix*, Table S5, $Eg5_{Sw1}$K146Q), we found that this mutation had no effect on steps 1 and 2 and only a minor effect on step 3. However, it reduces K_4 to a value essentially identical to that for kinesin 1. This indicates that a major effect of the mutation is to significantly increase the fraction of motors with Sw1 in a closed conformation after ATP hydrolysis. The value of k_4 at the temperature of our experiments (10 °C) (*SI Appendix*, Table S5) is slightly more than twice the rate constant for phosphate release measured at a higher temperature (7.9 ± 0.9 s^{-1} at 20 °C) (36), implying that this difference is considerably greater than twofold when comparing rate constants at the same temperature. We conclude from this that Sw1 reopening precedes the phosphate release step.

In our prior study (26), we examined how Sw1 and the NL are coordinated in Eg5 and kinesin 1 by monitoring the coupling ratio defined as the mole fraction of docked NL divided by the mole fraction of closed Sw1, and we calculated it from the evolution of corresponding TR^{2}FRET waveforms over time after mixing with ATP. A ratio of 1.0 implies tight NL/Sw1 coupling. For kinesin 1, this ratio is 0.99 in the absence of nucleotide (26). Mixing with 2 mM ATP causes the ratio to rise (Fig. 3*A*, light gray), and fitting to a single-exponential rate equation (Fig. 3*A*, solid black line) yields a rate constant of 32.3 ± 0.5 s^{-1} and a final coupling ratio of 2.1. By contrast, the coupling ratio for Eg5 (Fig. 3*A*, dark gray) is 0.29 in the absence of nucleotide (*SI Appendix*,

Table S4), and fitting the data subsequent to mixing with 2 mM ATP yields a rate constant of 3.8 ± 0.1 s^{-1} and an extrapolated coupling ratio of 7.9 (Fig. 3*A*, solid black curve). The rate constants for both kinesin 1 and Eg5 are consistent with the values of k_{cat} at the temperature of this experiment (10 °C). We interpret this to mean that, for kinesin 1, Sw1 and the NL are tightly coupled through ATP binding and hydrolysis—when NL docking occurs—and remain moderately coupled with entry into the steady state. By contrast, Sw1 and the NL for Eg5 are poorly coupled in the absence of nucleotide. Coupling improves with ATP binding and hydrolysis, but Sw1 and the NL become markedly uncoupled again with entry into the steady state. We performed a similar analysis on the K146Q mutant as well as on a second mutant (K146M), which provides an additional way of testing the importance of the α1-α2b salt bridge in Eg5 function; as in our prior study (26), we plotted the evolution of the coupling ratio over time from the TR^2FRET waveforms that are illustrated in Fig. 2. The plot of coupling ratio vs. time after mixing with 2 mM ATP is depicted in Fig. 3*B* for the K146Q (Fig. 3*B*, red) and K146M (Fig. 3*B*, magenta) constructs. Coupling ratios for these two constructs in the absence of nucleotide are 0.63 and 1.02 for K146Q and K146M, respectively. After mixing with ATP, this increases for both mutants, and fitting to the same rate equation (Fig. 3*B*, solid black lines) reveals rate constants and final coupling ratios of 4.2 ± 0.1 s^{-1} and 3.4 for K146Q and 4.1 ± 0.1 s^{-1} and 2.1 for K146M. We interpret these data to imply that two Eg5 mutations that abolish the α1-α2b salt bridge enhance NL/Sw1 coupling to levels that resemble kinesin 1.

In kinesin 1, the position of the NL regulates the kinetics of ATP hydrolysis—a process that depends, in turn, on the structure of Sw1 (37). In such a highly coupled system, load could thereby regulate the ATPase cycle of this motor. Since the K146Q mutation increases the conformational coupling between Sw1 and the NL, we might expect that it would also alter the load dependence of the motor mechanochemical ATPase cycle. We, therefore, next examined how load affects the mechanics of the K146Q acetylation mimetic at the single-molecule level.

Single-Molecule Mechanics Reveal That the K146Q Mutation Alters Motor Function Under Load. The function of single Eg5 motors was characterized via a standard optical trap bead assay (38–40). Because WT Eg5 run lengths are short, it is difficult to turn off the optical trap before bead detachment. Thus, to characterize unperturbed motion, we used the weakest trap possible (<0.0005 pN nm^{-1}) and left it on, allowing Eg5-driven beads to walk out of the trap. The maximum force that these motors experienced was about 0.07 pN at a position 150 nm from the trap center. Higher trap strengths were then used to characterize the response of the motors to load. We first tested a dimeric construct ("D"), consisting of the cys-light Eg5 motor domain, NL, and neck coiled coil (human Eg5 residues 1–402), fused to the kinesin 1 hinge and coiled coil (human kinesin 1 residues 372–560). As noted in prior studies (41, 42), fusion to the kinesin 1 coiled coil tail is necessary to generate dimeric constructs containing the Eg5 motor domain that produce appreciable run lengths. We compared the in vitro single-molecule mechanics of D with corresponding studies of a dimer that also contains the K146Q mutation (referred to herein as DK146Q). Consistent with prior studies (26, 43), we observed that D, like a WT Eg5 dimer, is quite insensitive to load, with single motors moving through a moderate-power optical trap at approximately constant velocity, although load increases as the motor moves away from the trap center (44). Here, we carried out a more systematic set of measurements to determine the force–velocity curves for D (Fig. 4*A* and *SI Appendix*, Fig. S4). We found that D maintains an approximately constant velocity until ~2.25 pN. It is able to advance under higher load, although velocity decreases as the load increases beyond 2.25 pN (Fig. 4*A*). By contrast, the K146Q mutation increases the sensitivity to load, and a significant velocity decrease occurs by 1.75 pN and continues to decrease more substantially above this force. While moving quite slowly (Fig. 4*A*), the K146Q mutation also allows the motor to access higher forces. Overall, the distribution of force production is shifted to higher forces for the K146Q motor (Fig. 4*B* and *SI Appendix*, Fig. S5*A*), and the durations of force production are increased even more relative to the WT (*SI Appendix*, Figs. S4 and S5*A*). We think several effects contribute to this. First, the decreased probability of detachment leads to achievement of higher forces and longer runs. Second, the slower velocity under load increases the duration of runs. Third, the increased stall probability and duration of stalls both contribute to longer periods of force generation. Fig. 4*B* depicts the histogram from the "best" events, which will undercount the short duration events. An uncurated histogram of all events can be found in *SI Appendix*, Fig. S5*A*. We note that, in both cases, short runs, especially those with lower force production, are likely to be undetected, and therefore, the actual single-molecule experimental data likely contain more short events than are detected experimentally.

It has previously been shown (45, 46) that sensitivity of velocity to load leads to optimal load sharing. In a team of such motors moving under load, the leading motors feels increased force and slow down, allowing the trailing motors to catch up. This improves load sharing and system performance, assuming that the

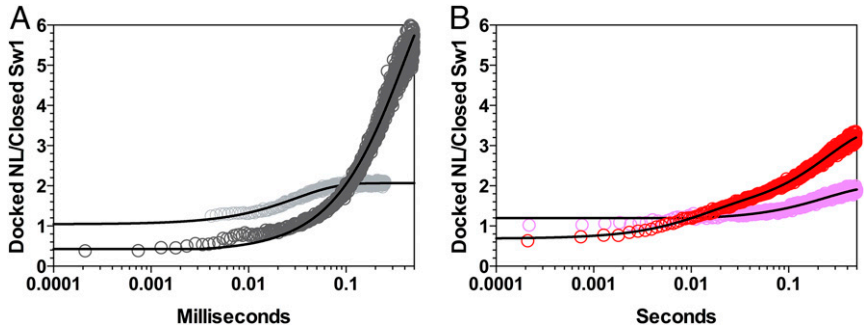

Fig. 3. Transient changes in NL/Sw1 coupling. (*A*) Plot of the coupling ratio defined as the ratio of mole fraction of docked NL to mole fraction of closed Sw1 vs. time after mixing Eg5 (dark gray) and kinesin 1 (light gray) Sw1 and NL FRET-labeled constructs with 2 mM ATP. A ratio of 1.0 implies tight conformational coupling of the NL to Sw1, with deviation in either direction implying looser coupling. Fitting to a single-exponential rate equation (solid black lines) yields rate constants and extrapolated coupling ratios described in the text. Data reproduced with permission from ref. 26. (*B*) Corresponding experiments for Eg5K146Q (red) and Eg5K146M (magenta). For both constructs, the coupling ratio resembles kinesin 1 more than unmodified Eg5.

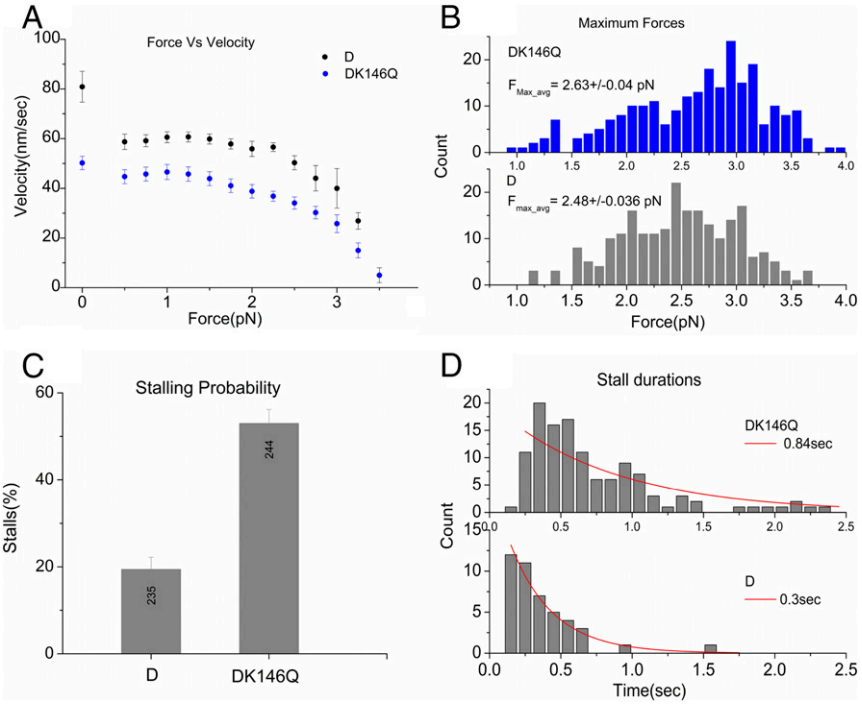

Fig. 4. Single-molecule force–velocity curves for dimeric Eg5 constructs. (*A*) Force–velocity curves from experimental single-molecule data of D and DK146Q in bead assays. Compared with the D dimer, the K146Q-modified dimer shows increased sensitivity to load, with a slower velocity at all loads tested. (*B*) Maximum forces and durations for D and DK146Q single motor-containing beads (best 15 traces from each single motor-containing bead). Overall, the distribution of force production is shifted to higher forces for the K146Q motor. (*C*) Stalling probabilities for D and DK146Q. (*D*) Stall durations for D and DK146Q single motor-containing beads.

forward motors do not detach prematurely. Consequently, we next examined the effect of load on the Eg5 detachment probability. We found that, for any given load, DK146Q has a lower probability of detachment than D (*SI Appendix*, Fig. S3*B*). We next examined the effect of the K146Q mutation on stall propensity and duration. To identify stalls, we used a 100-ms minimum cutoff and less than or equal to 0.5-pN change in average force. Statistical distributions of observed stalls suggested that DK146Q was much more likely to stall (Fig. 4*C*) and that it stalled for a much longer duration (Fig. 4*D*) than D. We also used a set of automated velocity-only criteria, where we looked at smoothed velocities of individual traces as a function of load, and determined the percentage of such traces with velocity that went below 20 nm/s at that load. At each load, we observed more extremely low-velocity traces (*SI Appendix*, Fig. S4*B*) for the K146Q mutant. Thus, as well as decreasing the probability of detachment under load, the K146Q mutation increases stall probability and duration as well as the overall duration of force production (*SI Appendix*, Fig. S4*A*). Since analyzing runs that display stalls potentially introduces a selection bias, we also compiled statistics on all recognizable runs using a 1-pN cutoff to avoid noise. The presence of the K146Q mutation shifts the entire population of events to higher forces of longer mean duration (*SI Appendix*, Fig. S5 *A* and *C*). In summary, our data imply that Eg5 motors acetylated at K146 are less likely to fall off the MT while under load and more likely to maintain higher forces for longer durations—features that would improve the summation of forces generated from multiple motors in an ensemble, enhancing overall system function.

To better understand how acetylation could affect motor function at the ensemble level, we used Monte Carlo simulations with motor parameters chosen from our single-molecule measurements (*SI Appendix*, Figs. S4, S6, and S7). These revealed improved ensemble force production in the K146Q mutant, which was reflected in larger mean forces, longer duration events, and an improved ability to escape from a fixed position optical trap (Fig. 5). This effect is progressively enhanced as the number of motors increases (compare Fig. 5 *A*, row 4 and *B*, left bars with Fig. 5 *A*, row 1 and *B*, right bars). During metaphase, Eg5 works in large ensembles in a "tug of war" with cytoplasmic dynein. Our results suggest that, in the presence of opposing load, Eg5 acetylation will cause the motor to slow down—unlike WT Eg5. This effect along with its enhanced ability to stall mean that acetylated Eg5, even when present in low concentrations, will act as a "brake" by interfering with nonacetylated Eg5 motors. We, therefore, predict that expression of low molar fractions of the K146Q acetylation mimetic in cells will slow spindle separation during metaphase. To test this, we next examined the effect of the K146Q mutation on spindle dynamics in cells.

Expression of the K146Q Acetylation Mimetic Reduces Spindle Pole Separation Velocity in Mitotically Active Cells. To assess the functional consequence of K146 acetylation, mCherry (mCh)-tagged full-length WT or K146Q Eg5 protein was expressed in HeLa cells. Based on quantitative Western blot analyses, we estimate that mCh-tagged Eg5 proteins were present at ~25% of the level of endogenous Eg5 (*SI Appendix*, Fig. S7 *A* and *B*). Importantly, both WT and K146Q versions of the motor localized to the mitotic spindle in metaphase cells (Fig. 6*A*). Measurements of mCh fluorescence along the pole to pole axis indicated that the spindle distribution of mCh-Eg5 K146Q did not differ from that for mCh-Eg5 WT (Fig. 6*B*). To compare the functional activity of the WT and K146Q Eg5, HeLa cells expressing GFP-tubulin and equivalent levels of mCh-Eg5 WT or mCh-Eg5 K146Q were treated with the Eg5 inhibitor monastrol, resulting in mitotic arrest and the formation of monopolar spindles (Fig. 6 *C* and *D*). Bipolar spindle formation was then measured after monastrol washout (Fig. 6*C* and Movies S1 and S2). Spindle lengths at the

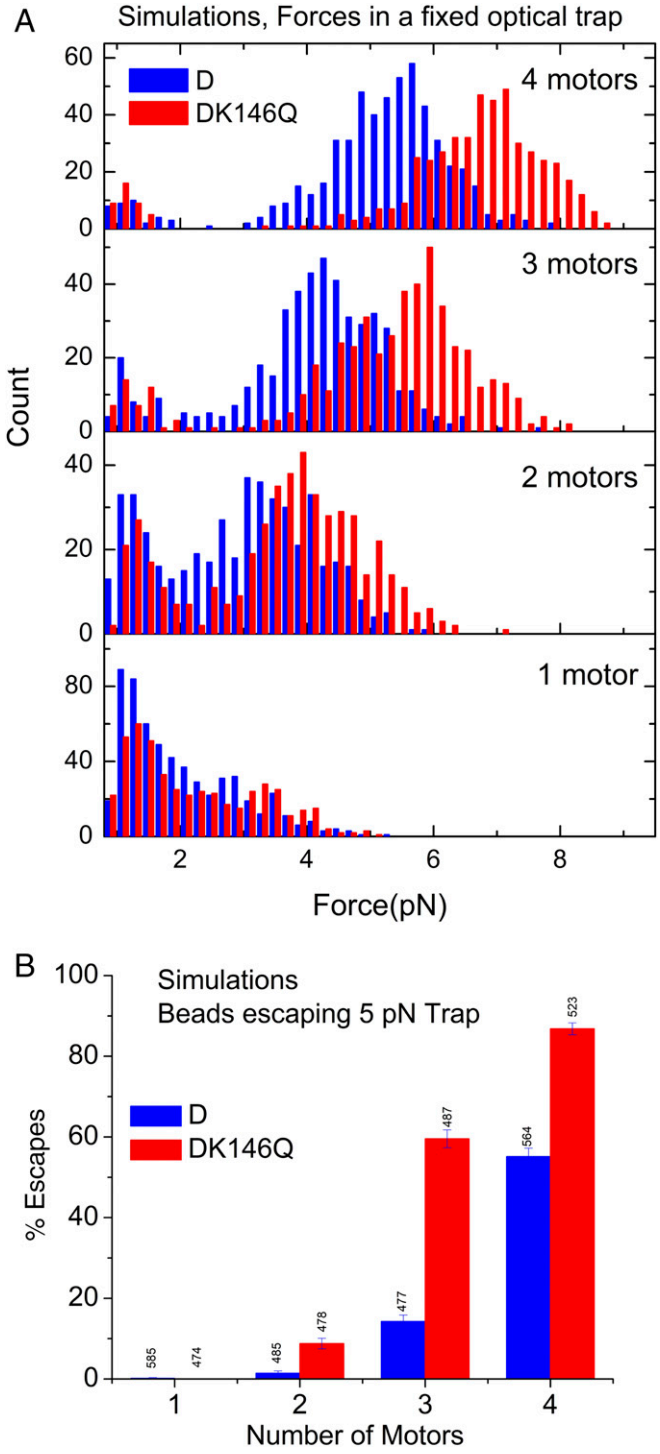

Fig. 5. Simulated forces and escape percentages for dimeric Eg5 constructs. (*A*) Monte Carlo simulations of forces as a function of increasing number of D and DK146Q dimers on a bead moving in a fixed strength optical trap (4.5 pN/100 nm). Simulations are carried out using forces and detachment probabilities derived from single-motor experiments (Fig. 4). Notice the shifts toward higher values for the K146Q mutant. (*B*) Escape percentages from a fixed strength optical trap simulated using forces and detachment probabilities derived from single-motor experiments (Fig. 4).

completion of pole separation were similar in cells expressing mCh-Eg5 WT or K146Q (11.02 ± 0.29 μm WT, 10.87 ± 0.26 μm K146Q, mean ± SEM) (Fig. 6*E*). However, pole separation occurred at a significantly slower velocity in cells expressing mCh-Eg5 K146Q (0.84 ± 0.07 μm/min) than in cells expressing mCh-Eg5 WT (1.35 ± 0.15 μm/min, $P = 0.0009$, unpaired t test) (Fig. 6*F*). Furthermore, expression of mCh-Eg5 WT did not alter pole separation velocity compared with control cells expressing mCh-tubulin (*SI Appendix*, Fig. S7*C*). Taken together, these data indicate that low levels of Eg5-K146Q in mitotic cells can act as a brake to slow spindle pole separation.

Acetylation of K146 in Eg5 Is Present in Low Abundance in Tumor Cell Lysates and Can Occur Nonenzymatically. Although acetylation of K146 in Eg5 has been repeatedly observed in the literature (15–17), we wished to determine how abundant this modification is in interphase cells. We, therefore, generated lysates from two primary patient-derived glioma xenografts, immunoprecipitated Eg5, treated the SDS/PAGE-resolved Eg5 band to tryptic and chymotryptic digestion, and subjected the resulting peptides to liquid chromatography-tandem mass spectrometry (LC-MS/MS) analysis. The resolved peptides covered ∼65–85% of the total protein sequence. In particular, a chymotryptic digest revealed a low-abundance peptide (∼ 0.6%) with a collision-induced dissociation spectrum that is shown in *SI Appendix*, Fig. S8. The mass of this ion is consistent with the acetylated form of the EKLTDNGTEF peptide, and the mass difference between the y9 and y8 ions in this spectrum is consistent with acetylation at K146.

There are at least 17 lysine acetyl transferases (47) that catalyze the nucleophilic attack by the ε-amino group of protein lysines onto acetyl CoA to generate the acetylated PTM. However, lysine acetylation can also occur nonenzymatically in cells (48–50). We wished to expose Eg5 to conditions conducive to nonenzymatic acetylation as a means to determine if K146 is sufficiently surface exposed for this modification to occur and to further support our in vivo finding. We, therefore, incubated dimer D with 1 mM acetyl CoA at room temperature at pH 7.5 for 12 h and subjected the material to LC-MS/MS analysis, comparing our results with those of a control D sample that was not exposed to acetyl CoA. Results are summarized in *SI Appendix*, Fig. S10. D contains the first 401 residues from Eg5, and we concentrated our analysis on this portion of the chimera. Samples were subjected to tryptic and chymotryptic digestion, and the resulting peptides covered ∼80–95% of the protein sequence. While the first 401 residues of D contain 31 lysines, we could detect acetylation in only 10 of these, including K146, which was identified in two peptides. No acetylated peptides could be detected in the control samples. The K^{acetyl}/K ratio for peptides containing K146 was ∼2.5%.

Discussion

Multiple Elements of the Cytoskeleton Are Subject to Posttranslational Modifications. Components of both the actomyosin and MT cytoskeleton are frequently modified posttranslationally (51–53). The role of PTMs in regulating MT dynamics and function plays a central role in regulating MT function and has been referred to as the "tubulin code" (7–9). By comparison, less is known about the roles that PTMs have on kinesin function, and even less still is known about their effects on motor function. In kinesin 1, serine 175, at the amino-terminal end of the α3 helix, can be phosphorylated by the JNK3 kinase, which reduces stall force by 20% (54). A recent report has also described *src*-mediated phosphorylation of tyrosine residues in the motor domain of Eg5, including those located in the α3 helix and in Loop 5—in close proximity to residue K146 (12). However, these studies do not provide insight into how PTMs alter motor mechanochemistry. Furthermore, these modifications all reduce motor function—acting in essence as "on/off" switches. In our prior studies of Eg5 (26, 36), we showed that Loop 5, which splits the α2 helix into α2a (N terminus) and α2b (C terminus), functions in part by regulating the conformational

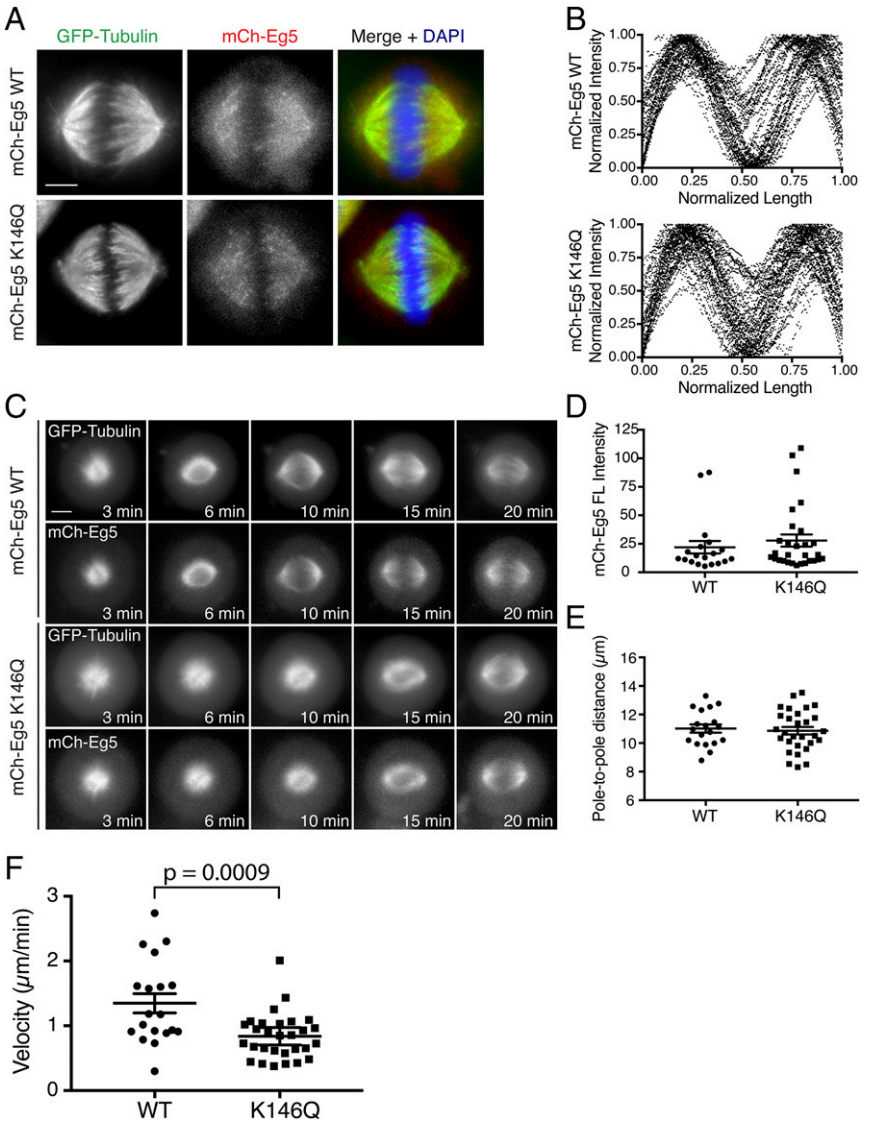

Fig. 6. Expression of mCh-Eg5 K146Q slows pole separation during spindle formation. (*A*) Full-length mCh-Eg5 WT and mCh-Eg5 K146Q (red) localize to the mitotic spindle (green). (Scale bar: 5 μm.) (*B*) mCh-Eg5 WT (*Upper*) and mCh-Eg5 K146Q (*Lower*) are similarly distributed along the length of the spindle (n = 43 cells per mCh-Eg5 construct from three independent experiments). (*C*) Stills from representative time-lapse movies of cells expressing GFP-tubulin and the indicated mCh-Eg5 construct. Time stamps indicate time after monastrol washout. (Scale bar: 5 μm.) (*D*) Plot of mCh fluorescence levels for mCh-Eg5 WT- and mCh-Eg5 K146Q-expressing cells analyzed in *E* and *F*. (*E*) Plot of final spindle length at the conclusion of pole separation after monastrol washout (n = 19 mCh-Eg5 WT and n = 29 mCh-Eg5 K146Q cells from four independent experiments, P = 0.71 unpaired t test). (*F*) Plot of pole separation velocity in cells expressing mCh-Eg5 WT and mCh-Eg5 K146Q [1.35 ± 0.15 (mean ± SEM) WT vs. 0.84 ± 0.07 K146Q, n = 19 WT, n = 29 K146Q, P = 0.0009 unpaired t test].

coupling between the catalytic site and the NL and that a mutation at the junction of Loop 5 with α2b (P131A) had profound effects on this coupling. This motivated us to look for a well-documented PTM in α2b with local structural effects that could be predicted, and this, in turn, led us to examine the mechanochemical consequences of lysine 146 acetylation.

While acetylation has long been recognized as a PTM of histones (21, 55–59), it has been more recently appreciated that it also occurs in components found throughout the cell, including transcription factors, metabolic enzymes, and structural proteins (22–24). Our proteomics results show that acetylation of K146 can be detected in low abundance in nonsynchronized glioma cells. They also show that, in the motor domain and neck coiled coil of Eg5, only about 30% of lysine residues—including K146—are sufficiently reactive to undergo nonenzymatic acylation by acetyl CoA. In this study, we did not determine which lysine acetyl transferases are responsible for K146 acetylation or to what degree nonenzymatic acetylation occurs intracellularly. However, our results in *SI Appendix*, Fig. S9 show that K146 acylation can occur nonenzymatically, and if this turns out to be physiologically relevant, it raises the possibility that regulation of this PTM may occur at the level of deactylases. The low abundance of acetylated K146 that we observe in nonsynchronized tumor cells suggests either (*i*) that low levels of acetylated K146 Eg5 are sufficient to affect ensemble motor function—consistent with our finding that modification of only a minority of Eg5 is sufficient to significantly slow spindle pole separation—or (*ii*) that acetylation is a cell cycle -regulated event.

Disrupting the α1-α2b Salt Bridge in Eg5 Enhances Allosteric Communication Between the Catalytic Site and the NL. Our MD simulations predicted large-scale effects from eliminating the

α1-α2b salt bridge. This includes increased interactions and conformational couplings between α1, β7, the CS, L13, and the NL as well as between α0, the P loop, and Sw1 (Fig. 1 and *SI Appendix*, Tables S2 and S3). In particular, a cluster of charged residues, including E92 (α1), K17 (CS), K362 (NL), and R329 (Loop 13), displays increased interactions on salt bridge disruption that together maintain the CS and NL in a state that is more frequently coordinated and docked. Metadynamics simulations also revealed an enhanced NL docking potential for the mutant (Fig. 1*C*). In concert with these changes, Sw1 more frequently adopts a closed conformation due primarily to increased Loop 9, α0, and P-loop coordination. Collectively, these results suggest that acetylation of K146 produces a motor where nucleotide binding/hydrolysis and NL docking are tightly coupled. Loose coupling in unmodified Eg5 would prevent one motor from acting as a brake that could slow or stop other motors in the ensemble. However, in some circumstances, Eg5 tonically opposes the effects of cytoplasmic dynein, and under these conditions, there may be a need for Eg5 to act more like kinesin 1—stalling rather than dissociating. Utilizing TR^2FRET, we have found that both the K146Q and K146M acetylation mimetics accelerate ATP-induced NL docking 2.2- to 3.4-fold (Fig. 2 *C* and *E* and *SI Appendix*, Fig. S10 and Table S4) and enhance the mole fraction of closed Sw1 after ATP hydrolysis (Fig. 2*D* and *SI Appendix*, Table S4). This ensures that Sw1 and the NL remain conformationally coupled through ATP hydrolysis and P_i release, when the power stroke occurs, and indicates that K146 acetylation makes Eg5 resemble kinesin 1. In a prior study (26), we observed that, when Sw1 in Eg5 is closed, it stabilizes Sw2 into a strong MT binding conformation. The increased mole fraction of closed Sw1 that we observe with the K146Q mutant after ATP hydrolysis (step K_4; above) implies that acetylation should enhance the fraction of the time that the motor is strongly bound to the MT. Taken together, our MD and TR^2FRET studies predict that the consequences of K146 acetylation should be particularly apparent under load, and our single-molecule mechanics studies confirm this.

Unlike other kinesin PTMs, K146 acetylation produces a "gain in function," which enhances Eg5's ability to work in teams to overcome dynein-produced opposing load. At the single-molecule level, there are four qualitative changes. First, detachment under load is decreased (*SI Appendix*, Fig. S4*B*), and therefore, single motors reach higher forces (Fig. 5 and *SI Appendix*, Figs. S4 and S6). Second, the probability to transition into a "stalled" state increases threefold (Fig. 5). This favors multiple motor load sharing. Third, the duration of stalls is longer (Fig. 5), which means that acetylated motors remain attached and provide other motors more time to attach and contribute to ensemble function. Fourth, even when such motors do not stall, they are more slowed down by load (Fig. 5 and *SI Appendix*, Fig. S3), which means that they spend more time supporting higher loads before detaching. These effects lead to better ensemble motor function under load (Fig. 6 and *SI Appendix*, Fig. S6), and the capabilities that they provide Eg5 are remarkably similar to those provided for dynein by its cofactors NudE and Lis1. NudE and Lis1 alter dynein detachment kinetics under load, with individual dynein motors holding on to MTs longer, allowing better group function as motors share load and enabling the complex to transport a cargo against significant opposition (60, 61). Remarkably, acetylation of K146 does essentially the same thing for Eg5. On average, dynein with Lis1 and NudE holds on to MTs 60% longer before detaching compared with dynein alone (60), an effect of comparable magnitude to what we observed in the K146Q mutation. This seems to be a form of convergent evolution, and it implies that the ability to modulate a motor's performance under load is an important variable for multiple molecular motors, regardless of their evolutionary source.

Disrupting the α1-α2b Salt Bridge Alters Eg5 Mitotic Function. By increasing conformational coupling and the lifetime of strong MT binding states, the K146Q acetylation mimetic mutation alters the force–velocity landscape of Eg5 so as to enhance motor efficiency in ensembles, reduce velocity in the presence of opposing load, and increase the probability of stalling. This would enable modified Eg5 to act as a brake, slowing centrosome separation by generating drag force against unmodified Eg5 motors. Spindle function involves a complex orchestration of multiple motors that, during at least part of the spindle lifetime, work in opposition to each other, and fine tuning of motor mechanical output is necessary to fine tune this balance of forces. While ubiquitination and proteolysis of mitotic kinesins are a well-recognized form of regulation, this seems unlikely to enable the cell to adjust motor output on the moment by moment basis that may be needed to balance opposing forces. Our biophysical results predict that acetylation of only a fraction of Eg5 is capable of slowing centrosome separation, and we observed this in our time-lapse microscopy studies (Fig. 6).

Eg5 is a member of the kinesin 5 family of mitotic motors, and we note that at least one other member of this family—BMK-1 from *Caenorhabditis elegans*—has also been reported to act as a spindle brake (62). Unlike Eg5, BMK-1 is not essential for mitosis or normal development. Its deletion accelerates spindle pole separation over twofold, implying that it provides a force that opposes spindle elongation. Alignment of the BMK-1 sequence with that for Eg5 reveals that the α1-α2b salt bridge seen in the latter is absent in the former. In particular, Eg5 residues D91 (α1) and K146 (α2b) are replaced in BMK-1 by residues K83 and Q136, respectively. Our results in conjunction with this prior work imply that there is an evolutionarily conserved need for some kinesin 5 motors to act for at least part of the cell cycle as a brake and that this need in some organisms is served by synthesis of a nonessential kinesin 5, while in others, it is served through a reversible PTM that provides cells with functional flexibility.

K146 Acetylation Highlights the Importance of the α1-α2b Salt Bridge in Tuning the Mechanochemical Properties of Kinesins. That both the K146Q and K146M mutations have very similar effects on conformational coupling implies that the effects of these mutations—and of the K146 acetylation, which these mutants mimic—are due to loss of the α1-α2b salt bridge and not to side chain interactions requiring acetyl lysine. The increased conformational coupling that we observe with both the mutations is largely a result of the threefold acceleration of NL docking, which allows this process to track with Sw1 closure. Our work, therefore, leads us to predict that NL docking should be relatively slow for kinesins with an α1-α2b ionic bond and appreciably faster in kinesins that lack it. This prediction is consistent with the limited set of data on the kinetics of NL docking, which shows that it is slow in both Eg5 (60–80 s^{-1} at 20 °C) (27) and CENP-E (~29 s^{-1} at 20 °C) (63). Both of these motors contain an α1-α2 salt bridge, with D91 and K146 in Eg5 corresponding to D72 and K116 in CENP-E (64). By contrast, kinesin 1 is devoid of this ionic interaction (65). We would, therefore, predict a priori that NL docking in kinesin 1 should be faster than in WT Eg5 or CENP-E, and in fact, it is (>800 s^{-1} at 20 °C) (66). Critically testing the relationship between the α1–α2b interaction and NL docking kinetics will require additional comparisons with other kinesins. Two examples could serve as the basis for future studies. First, we note that Kif15, another mitotic kinesin, is also devoid of an α1-α2 salt bridge (67), and our results would predict that NL docking should be rapid. Second, at least one other kinesin (Kif22) has a documented PTM in α2b (68, 69)—phosphorylation of T158, corresponding to position 147 in Eg5. Phosphorylated T158 could make a salt bridge with arginine 113,

corresponding to residue D91 in Eg5. It seems likely that the approach that we have utilized in our study of K146 acetylation in Eg5 should be readily applicable to elucidate the consequences of altering the interaction between α1 and α2 in these and other kinesins as well.

Materials and Methods

A complete discussion of all methods, including generation of the kinesin cysteine mutants, expression, purification, ATPase assays, transient kinetic, methodologies, TR^2FRET data acquisition and analysis, proteomics analysis, cell transfection, and video microscopy, is included in *SI Appendix*.

ACKNOWLEDGMENTS. We thank Dr. Xin-Qiu Yao (University of Michigan) for valuable discussions and simulation analysis assistance. This work was supported by American Heart Association Grant 14SDG20480032 (to J.M.M.); NIH Grants AR032961 (to D.D.T.), GM121491 (to J.S.), GM070862 (to B.J.G.), GM123068 (to S.P.G.), GM102875 (to S.S.R.), and NS073610 (to S.S.R.); and Susan G. Komen Grant CCR16377648 (to J.S.). The Orbitrap Elite instrument used in this study was purchased via NIH Shared Instrument Grant 1S10RR031537-01.

1. Hirokawa N, Tanaka Y (2015) Kinesin superfamily proteins (KIFs): Various functions and their relevance for important phenomena in life and diseases. *Exp Cell Res* 334:16–25.
2. Vicente JJ, Wordeman L (2015) Mitosis, microtubule dynamics and the evolution of kinesins. *Exp Cell Res* 334:61–69.
3. Bachmann A, Straube A (2015) Kinesins in cell migration. *Biochem Soc Trans* 43:79–83.
4. Walczak CE, Gayek S, Ohi R (2013) Microtubule-depolymerizing kinesins. *Annu Rev Cell Dev Biol* 29:417–441.
5. Jolly AL, et al. (2010) Kinesin-1 heavy chain mediates microtubule sliding to drive changes in cell shape. *Proc Natl Acad Sci USA* 107:12151–12156.
6. Braun A, et al. (2014) Rac1 and Aurora A regulate MCAK to polarize microtubule growth in migrating endothelial cells. *J Cell Biol* 206:97–112.
7. Yu I, Garnham CP, Roll-Mecak A (2015) Writing and reading the tubulin code. *J Biol Chem* 290:17163–17172.
8. Janke C (2014) The tubulin code: Molecular components, readout mechanisms, and functions. *J Cell Biol* 206:461–472.
9. Sirajuddin M, Rice LM, Vale RD (2014) Regulation of microtubule motors by tubulin isotypes and post-translational modifications. *Nat Cell Biol* 16:335–344.
10. Hornbeck PV, et al. (2015) PhosphoSitePlus, 2014: Mutations, PTMs and recalibrations. *Nucleic Acids Res* 43:D512–D520.
11. Liu Z, et al. (2014) CPLM: A database of protein lysine modifications. *Nucleic Acids Res* 42:D531–D536.
12. Bickel KG, et al. (2017) Src family kinase phosphorylation of the motor domain of the human kinesin-5, Eg5. *Cytoskeleton (Hoboken)* 74:317–330.
13. Falnikar A, Tole S, Baas PW (2011) Kinesin-5, a mitotic microtubule-associated motor protein, modulates neuronal migration. *Mol Biol Cell* 22:1561–1574.
14. Venere M, et al. (2015) The mitotic kinesin KIF11 is a driver of invasion, proliferation, and self-renewal in glioblastoma. *Sci Transl Med* 7:304ra143.
15. Choudhary C, et al. (2009) Lysine acetylation targets protein complexes and co-regulates major cellular functions. *Science* 325:834–840.
16. Sol EM, et al. (2012) Proteomic investigations of lysine acetylation identify diverse substrates of mitochondrial deacetylase sirt3. *PLoS One* 7:e50545.
17. Nalawansha DA, Gomes ID, Wambua MK, Pflum MKH (2017) HDAC inhibitor-induced mitotic arrest is mediated by Eg5/Kif11 acetylation. *Cell Chem Biol* 24:481–492.e5.
18. de Boor S, et al. (2015) Small GTP-binding protein Ran is regulated by post-translational lysine acetylation. *Proc Natl Acad Sci USA* 112:E3679–E3688.
19. Gorsky MK, Burnouf S, Dols J, Mandelkow E, Partridge L (2016) Acetylation mimic of lysine 280 exacerbates human Tau neurotoxicity in vivo. *Sci Rep* 6:22685.
20. Cohen TJ, et al. (2011) The acetylation of tau inhibits its function and promotes pathological tau aggregation. *Nat Commun* 2:252.
21. Marmorstein R, Zhou MM (2014) Writers and readers of histone acetylation: Structure, mechanism, and inhibition. *Cold Spring Harb Perspect Biol* 6:a018762.
22. Menzies KJ, Zhang H, Katsyuba E, Auwerx J (2016) Protein acetylation in metabolism–Metabolites and cofactors. *Nat Rev Endocrinol* 12:43–60.
23. Kouzarides T (2000) Acetylation: A regulatory modification to rival phosphorylation? *EMBO J* 19:1176–1179.
24. Blee TK, Gray NK, Brook M (2015) Modulation of the cytoplasmic functions of mammalian post-transcriptional regulatory proteins by methylation and acetylation: A key layer of regulation waiting to be uncovered? *Biochem Soc Trans* 43:1285–1295.
25. Xie Y, et al. (2015) Posttranslational modification of autophagy-related proteins in macroautophagy. *Autophagy* 11:28–45.
26. Muretta JM, et al. (2015) The structural kinetics of switch-1 and the neck linker explain the functions of kinesin-1 and Eg5. *Proc Natl Acad Sci USA* 112:E6606–E6613.
27. Rice S, et al. (1999) A structural change in the kinesin motor protein that drives motility. *Nature* 402:778–784.
28. Gigant B, et al. (2013) Structure of a kinesin-tubulin complex and implications for kinesin motility. *Nat Struct Mol Biol* 20:1001–1007.
29. Cao L, et al. (2014) The structure of apo-kinesin bound to tubulin links the nucleotide cycle to movement. *Nat Commun* 5:5364.
30. Sindelar CV, Downing KH (2007) The beginning of kinesin's force-generating cycle visualized at 9-A resolution. *J Cell Biol* 177:377–385.
31. Rosenfeld SS, Xing J, Jefferson GM, King PH (2005) Docking and rolling, a model of how the mitotic motor Eg5 works. *J Biol Chem* 280:35684–35695.
32. Atherton J, Farabella I, Yu IM, Rosenfeld SS, Houdusse A, Topf M, Moores CA (2014) Conserved mechanisms of microtubule-stimulated ADP release, ATP binding, and force generation in transport kinesins. *Elife* 3:e03680.
33. Goulet A, et al. (2014) Comprehensive structural model of the mechanochemical cycle of a mitotic motor highlights molecular adaptations in the kinesin family. *Proc Natl Acad Sci USA* 111:1837–1842.
34. Goulet A, et al. (2012) The structural basis of force generation by the mitotic motor kinesin-5. *J Biol Chem* 287:44654–44666.
35. Hwang W, Lang MJ, Karplus M (2008) Force generation in kinesin hinges on cover-neck bundle formation. *Structure* 16:62–71.
36. Behnke-Parks WM, et al. (2011) Loop L5 acts as a conformational latch in the mitotic kinesin Eg5. *J Biol Chem* 286:5242–5253.
37. Clancy BE, Behnke-Parks WM, Andreasson JOL, Rosenfeld SS, Block SM (2011) A universal pathway for kinesin stepping. *Nat Struct Mol Biol* 18:1020–1027.
38. Block SM, Goldstein LS, Schnapp BJ (1990) Bead movement by single kinesin molecules studied with optical tweezers. *Nature* 348:348–352.
39. Li Q, King SJ, Gopinathan A, Xu J (2016) Quantitative determination of the probability of multiple-motor transport in bead-based assays. *Biophys J* 110:2720–2728.
40. Jun Y, Tripathy SK, Narayanareddy BRJ, Mattson-Hoss MK, Gross SP (2014) Calibration of optical tweezers for in vivo force measurements: How do different approaches compare? *Biophys J* 107:1474–1484.
41. Düselder A, Thiede C, Schmidt CF, Lakämper S (2012) Neck-linker length dependence of processive Kinesin-5 motility. *J Mol Biol* 423:159–168.
42. Lakämper S, et al. (2010) The effect of monastrol on the processive motility of a dimeric kinesin-5 head/kinesin-1 stalk chimera. *J Mol Biol* 399:1–8.
43. Valentine MT, Fordyce PM, Krzysiak TC, Gilbert SP, Block SM (2006) Individual dimers of the mitotic kinesin motor Eg5 step processively and support substantial loads in vitro. *Nat Cell Biol* 8:470–476.
44. Shojania Feizabadi M, et al. (2015) Microtubule C-terminal tails can change characteristics of motor force production. *Traffic* 16:1075–1087.
45. Mallik R, Petrov D, Lex SA, King SJ, Gross SP (2005) Building complexity: An in vitro study of cytoplasmic dynein with *in vivo* implications. *Curr Biol* 15:2075–2085.
46. Kunwar A, Vershinin M, Xu J, Gross SP (2008) Stepping, strain gating, and an unexpected force-velocity curve for multiple-motor-based transport. *Curr Biol* 18:1173–1183.
47. Allis CD, et al. (2007) New nomenclature for chromatin-modifying enzymes. *Cell* 131:633–636.
48. Wagner GR, Payne RM (2013) Widespread and enzyme-independent Nε-acetylation and Nε-succinylation of proteins in the chemical conditions of the mitochondrial matrix. *J Biol Chem* 288:29036–29045.
49. Wagner GR, Hirschey MD (2014) Nonenzymatic protein acylation as a carbon stress regulated by sirtuin deacylases. *Mol Cell* 54:5–16.
50. Pietrocola F, Galluzzi L, Bravo-San Pedro JM, Madeo F, Kroemer G (2015) Acetyl coenzyme A: A central metabolite and second messenger. *Cell Metab* 21:805–821.
51. Buss F, Kendrick-Jones J (2008) How are the cellular functions of myosin VI regulated within the cell? *Biochem Biophys Res Commun* 369:165–175.
52. Terman JR, Kashina A (2013) Post-translational modification and regulation of actin. *Curr Opin Cell Biol* 25:30–38.
53. Skoumpla K, Coulton AT, Lehman W, Geeves MA, Mulvihill DP (2007) Acetylation regulates tropomyosin function in the fission yeast Schizosaccharomyces pombe. *J Cell Sci* 120:1635–1645.
54. DeBerg HA, et al. (2013) Motor domain phosphorylation modulates kinesin-1 transport. *J Biol Chem* 288:32612–32621.
55. Shilatifard A (2006) Chromatin modifications by methylation and ubiquitination: Implications in the regulation of gene expression. *Annu Rev Biochem* 75:243–269.
56. Verdone L, Caserta M, Di Mauro E (2005) Role of histone acetylation in the control of gene expression. *Biochem Cell Biol* 83:344–353.
57. Forsberg EC, Bresnick EH (2001) Histone acetylation beyond promoters: Long-range acetylation patterns in the chromatin world. *BioEssays* 23:820–830.
58. Jenuwein T, Allis CD (2001) Translating the histone code. *Science* 293:1074–1080.
59. Reiner O, et al. (1993) Isolation of a Miller-Dieker lissencephaly gene containing G protein beta-subunit-like repeats. *Nature* 364:717–721.
60. McKenney RJ, Vershinin M, Kunwar A, Vallee RB, Gross SP (2010) LIS1 and NudE induce a persistent dynein force-producing state. *Cell* 141:304–314.
61. Reddy BJN, et al. (2016) Load-induced enhancement of Dynein force production by LIS1-NudE in vivo and *in vitro*. *Nat Commun* 7:12259.
62. Saunders AM, Powers J, Strome S, Saxton WM (2007) Kinesin-5 acts as a brake in anaphase spindle elongation. *Curr Biol* 17:R453–R454.
63. Rosenfeld SS, et al. (2009) The ATPase cycle of the mitotic motor CENP-E. *J Biol Chem* 284:32858–32868.
64. Garcia-Saez I, Blot D, Kahn R, Kozielski F (2004) Crystallization and preliminary crystallographic analysis of the motor domain of human kinetochore-associated protein CENP-E using an automated crystallization procedure. *Acta Crystallogr D Biol Crystallogr* 60:1158–1160.
65. Kull FJ, Sablin EP, Lau R, Fletterick RJ, Vale RD (1996) Crystal structure of the kinesin motor domain reveals a structural similarity to myosin. *Nature* 380:550–555.
66. Rosenfeld SS, Fordyce PM, Jefferson GM, King PH, Block SM (2003) Stepping and stretching. How kinesin uses internal strain to walk processively. *J Biol Chem* 278:18550–18556.
67. Klejnot M, et al. (2014) The crystal structure and biochemical characterization of Kif15: A bifunctional molecular motor involved in bipolar spindle formation and neuronal development. *Acta Crystallogr D Biol Crystallogr* 70:123–133.
68. Rigbolt KT, et al. (2011) System-wide temporal characterization of the proteome and phosphoproteome of human embryonic stem cell differentiation. *Sci Signal* 4:rs3.
69. Olsen JV, et al. (2010) Quantitative phosphoproteomics reveals widespread full phosphorylation site occupancy during mitosis. *Sci Signal* 3:ra3.